ANALYSIS OF LOAD FLOW AND STRESS CONCENTRATIONS IN TEXTILE COMPOSITES

Deepak Goyal*, John D. Whitcomb*, Julian Varghese*
***Department of Aerospace Engineering, Texas A&M University**
College Station, TX, USA 77840

Keywords: *textile composites, finite elements, load flow, stress concentrations, failure initiation*

Abstract

The increase in computational power has made three-dimensional analysis of textile composites practical. Interpretation of the results remains a challenge. Two non-standard techniques... calculation of stress resultants and stress volume distribution plots, were developed to transform massive amounts of output data into comprehensible modes of behavior. This study showed that in the warp tow of a plain weave, the maximum axial and transverse stress resultants occur at the maximum undulation region. An explanation of this behavior was proposed. The variation in transverse stress resultants was explained by using a simple stress transformation technique. The location of stress concentrations correlated with variation of the stress resultants. Stress volume distribution plots showed that some stress concentrations might be so localized that slight yielding might eliminate those stress concentrations. In comparable regions, the weaves studied showed similar variation in the axial and transverse stress resultants.

1 Introduction

Textile composites are being used in applications ranging from prostheses for amputees to shrouds to capture debris from a failed engine. Reduced part count, high speed textile preform manufacture, and increased damage tolerance due to the tow interlacing are the primary advantages of textile composites. There are many types of textile architectures, such as weaves, braids, and knits. For each type of architecture there are also many options. Optimal design through extensive experimental testing is not practical. Predictive tools are needed to perform virtual experiments of various options. Fortunately, the increase in computational power that is readily available is making detailed three-dimensional finite element analyses practical. One of the weak links in developing these models has been the difficulty in creating a finite element model. For this reason, initial efforts focused on the plain weave composite [1-2]. However, tools and techniques have improved and now 3D models have been developed for a variety of textiles (see Fig. 1).

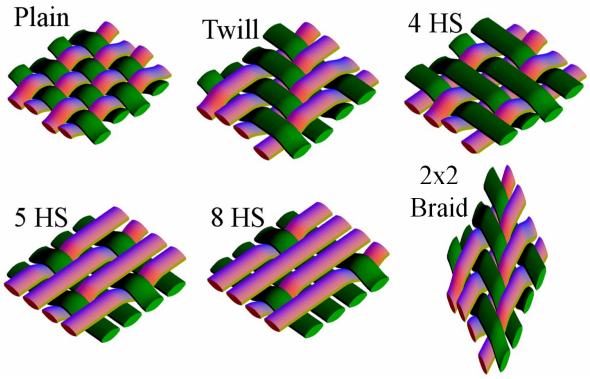

Fig. 1. Tow architecture of various textile composites (HS = harness satin)

The current 3D models of textile composites give much more information than the simple laminate theory models that were developed as part of the early efforts [3-4] to predict the behavior of woven composites. Ironically, in some ways the wealth of raw numerical information provided by the typical finite element analysis provides less basis for developing an intuitive understanding than the simpler models. The simple models represent the behavior in terms of a small number of basic modes of deformation and load transfer. Intuition is required to develop the models and the result is a framework for understanding the response. In contrast, finite elements models are based on very few preconceptions other than geometry… and the results are presented with similar lack of bias. For example, the stress contours for the normal stress σ_{11} in a 8 Harness Satin weave shown in Fig. 2 give many details, but no framework for interpretation.

The thesis of this paper is that optimal use of rapidly improving 3D finite element models requires non-standard techniques to interpret the data. (The

term "standard techniques" is defined herein to be postprocessing techniques available in commercial finite element programs). In particular, techniques must be developed that not only highlight the

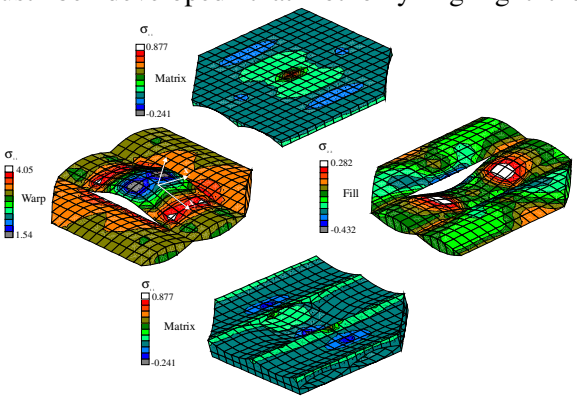

Fig. 2. Stress contours for 8-harness satin weave

important details, but also transform the massive amount of output data into comprehensible modes of behavior. This paper will discuss two techniques. The first technique is calculation of stress resultants that give forces and moments at any cross-section of the tow. The second technique converts the 3D variation of a stress component into a stress versus volume distribution plot. Both of the techniques will be described in detail.

These techniques were applied in various ways to investigate textile behavior. First, the behavior of a plain weave was analyzed. How the load flows along the various cross-sections of a plain weave and load distribution among warp, fill and matrix was investigated. It will be shown that in the warp tow, maximum axial and out of plane transverse stress resultants occur at the maximum undulation region. The reason for this will be discussed. The existence of out of plane transverse stress resultant will be explained by simple stress transformation. The location of stress concentrations will be correlated with stress resultants. Different architectures that were analyzed are Plain weave (PW), Twill weave, 4 Harness Satin weave (4HS), 5 Harness Satin weave (5HS) and 8 Harness Satin weave (8HS). Similar regions in these weaves were identified. The effect of tow architecture on the load flow in comparable regions of different weaves will be shown. The volume distribution plot will be used to show which stress components of a plain weave tow could initiate failure.

It should be noted that these postprocessing techniques are not meant to eliminate the details. Instead a hierarchical strategy is proposed that allows interpretation of the predictions at different levels of detail. Also, by providing the "coarse level" interpretation of the results, a better basis is provided for evaluating and refining simpler models.

2 Configurations

Five different weave architectures that were analyzed are PW, Twill weave, 4HS, 5HS and 8HS weaves. Their solid models and corresponding finite element models are shown in Fig. 1 and Fig. 3 respectively. Because the mats are symmetrically stacked, only one-half unit cells were modeled. By exploiting symmetries within these half unit cells, one could model smaller regions, but one half unit cells were employed here so that load flow and stress volume calculations could be conducted conveniently. Periodic boundary conditions were imposed on all the faces of the unit cell. The boundary conditions for different weave architectures are provided in detail in ref. [5]. The global coordinate system xyz (see Fig. 3) is shown for the Twill weave and lies at the similar location on the white boxes for other weaves too. Notice that except for PW, all the weaves have wavy (undulating) as well straight regions. The boundaries of the tow cross-section and the wavy part of the tow path can be described by a cosine function of the form:

$$z = \frac{h}{4}\cos\left(\frac{2\pi(s+s_0)}{\lambda}\right) + z_0 \qquad (1)$$

where s = x or y, s_0 and z_0 are offsets, h is the model thickness, and λ is the wavelength of the wavy region and was generally = 6 herein. Limited analyses were also performed for plain weave configurations with higher waviness ratio. In those cases, the wavelength of the wavy region λ was 3. Comparable regions in different weaves were identified and are also shown in Fig. 3. Comparable regions contain only undulating portion of the warp tow and fill tows plus the matrix pockets. The comparable regions in different weaves are marked by white boxes. They contain the whole thickness (h) of the model and vary from x=0 to x= λ/2 and y= -λ/4 to y=λ/4 (see Fig. 3) in each weave. The comparable regions without the matrix pockets are shown in Fig. 3(b). The weaves consisted of S2 glass and SC-15 resin. The material properties are given in Table 1. The fiber volume fraction in the tow was 78%. The tow fraction in the model was 63.6%, hence the overall fiber volume fraction in each model was 50%. The strength values for the tow were obtained based on the analytical formulas given by Chamis [6]. A volume averaged stress $\langle\sigma_{xx}\rangle$=1 was applied to each model, unless specified otherwise.

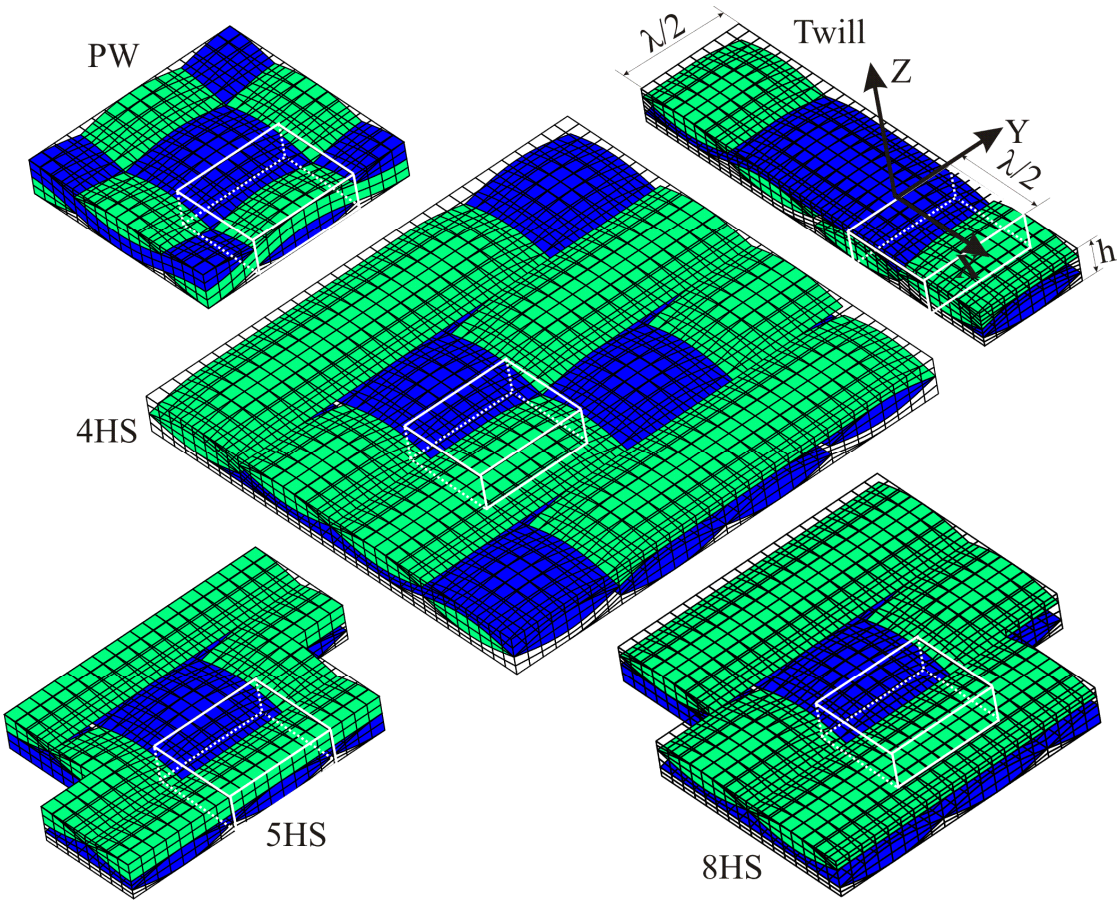

(a) Finite element meshes for half unit cells (comparable regions are marked by white boxes)

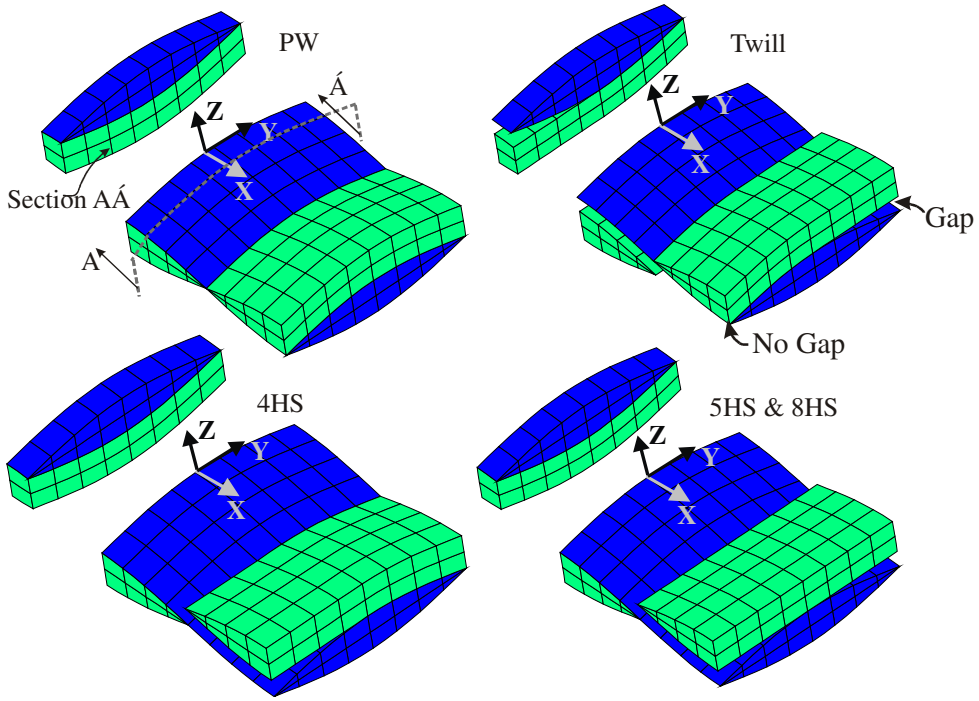

(b) Comparable regions (without the matrix pockets)
The layer of elements at x=0 is also shown detached to show gap between the tows

Fig. 3. FE meshes and comparable regions for different weave architectures.

Table 1. Material Properties of the tow & matrix

Moduli (GPa) & Poisson's ratios	Tow* S2 Glass/ SC-15	Matrix SC-15	Strengths (MPa)	Tow* S2 Glass/ SC-15
E_{11}	75.92	2.82	S_{11}	2861
$E_{22} = E_{33}$	22.98	2.82	$S_{22} = S_{33}$	53
$G_{12} = G_{13}$	7.16	1.01	$S_{12} = S_{13}$	48.3
G_{23}	8.26	1.01	S_{23}	31.2
$\nu_{12} = \nu_{13}$	0.26	0.395	S^c_{11}	2861
ν_{23}	0.39	0.395	$S^c_{22} = S^c_{33}$	53

*Fiber volume fraction in tow = 78%, ^{c} = compressive

3 Description of Postprocessing techniques

In this section, two post processing techniques that are used to interpret the FE analysis data are discussed. The first technique converts the 3D variation of a stress component into a stress versus volume distribution plot. This kind of plot reveals how much volume of the material has a stress magnitude larger than a particular value. The plot gives a measure of the non-uniformity of the stress distribution. This is especially useful for assessing whether a local stress concentration is so localized that slight yielding will eliminate the high stress. More details and usage of this technique will be discussed in the results section.

The other technique is the calculation of stress resultants. In approximate models, the components of the textile are treated as simple structural elements like rods or beams and stress resultants are used to describe the load flow. The fully three-dimensional finite element results can be post-processed to obtain stress resultants, such as the axial force or moment acting at any cross-section of the tow or matrix. The concept is illustrated for a cross-section *abcd* of the warp tow in Fig. 4. The nodal forces on the nodes lying on cross-section *abcd* can be calculated during the finite element analysis. We used 20 node brick elements, therefore each element has 60 forces, 3 at each node in x, y and z direction. These are labeled as fx, fy and fz respectively and are shown in Fig. 4 for one node.

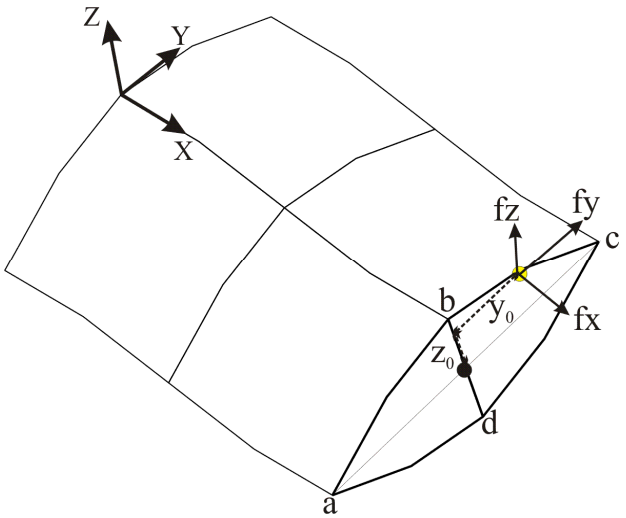

Fig. 4. Stress resultants at cross-section abcd

The forces Fx, Fy and Fz on a particular cross-section are simply the summation of all the nodal forces on that cross-section in the x, y and z directions respectively. At each cross-section, the moments about the cross-section centroid due to the nodal forces were calculated. The moments about the x, y, and z-axes are defined to be Rx, Ry, and Rz, respectively. Since stress resultants are obtained from full 3D models, the results are much more reliable than one could obtain by using a simplified model. Use of this technique to post process the finite element data will be shown in the results sections.

It should be noted that cross-section *abcd* is the interface between two layers of elements. The magnitude of forces and moments acting on cross-section *abcd* calculated from the left layer of elements will not be equal to that calculated from the right layer because due to tow undulation, the stress state is different in the two layers of elements. But if the layer thickness is reduced, the difference between the forces on the left and right should decrease. The hypothesis was found to be true by considering meshes with different refinement. Figure 5 shows smaller regions of different meshes of a PW with 4, 12, 24 and 48 cross-sections. The maximum difference between Fx calculated from the left layer of elements and right layer of elements for the warp tow was 2.65, 1.38, 0.81 and 0.46% for meshes with 4, 12, 24 and 48 cross-sections respectively. Hence, as the number of cross-sections increased, the difference between the magnitudes of forces calculated from the left and right layers of elements decreased. In the results that follow, 4 sections meshes were used to keep the runtimes low. The average forces or stress resultants were used in the analyses and were calculated by averaging the magnitudes of forces from the left and right layers of elements. Maximum difference between the average forces calculated using 4 sections meshes and those calculated using 48 section meshes was less than 3%.

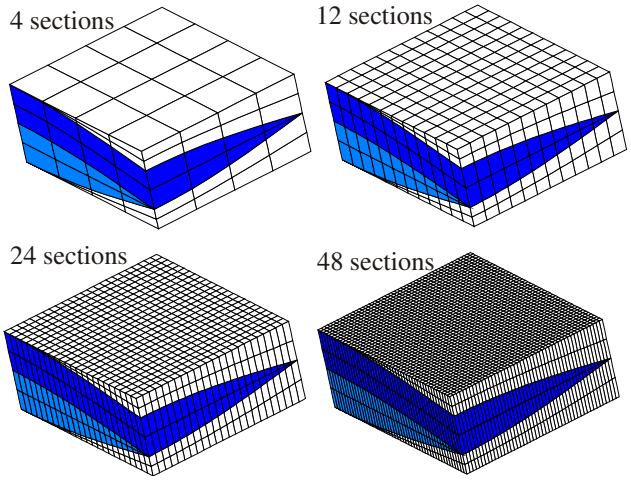

Fig. 5. Meshes used for convergence study

4 Results and Discussion

Special post processing techniques were applied to investigate textile behavior. Load flow and stress volume distribution plots were employed to understand the behavior of a plain weave. The effect of tow architecture on the load flow in comparable regions of different weaves was also investigated. The results are discussed below.

4.1 Analysis of a Plain Weave

First, a plain weave was analyzed for the load flow in the warp tow, fill tow and matrix pockets. The potential correlation between the stress concentrations and magnitudes of stress resultants in the warp tow was investigated. The load flow and stress distribution in the plain weave were also compared with that in a curved beam to obtain insights about the plain weave behavior. Typical stress volume distributions in the tow of a plain weave were also examined.

4.1.1 Load Flow in a Plain Weave

Uniaxial tensile load was applied to a PW along the x direction. Since the area of the cross-section is 3 and the applied volume averaged $<\sigma_{xx}>$ was 1, the total Fx force at any cross section of the model was 3. This causes considerable Fx and Fz stress resultants, but the Fy stress resultants were negligibly small. Figure 6 shows the Fx distribution in the warp tow, fill tow, matrix pockets and the total. The warp, fill and matrix do not have a uniform load flow, but the total is always constant. Both the warp tow and matrix have a peak where the crimp angle for the warp tow is maximum. The Fx in the warp tow increases by 23% from its value at x=0 and the corresponding peak in the matrix is around 8 times its value at x=0. In contrast, the fill tow has a

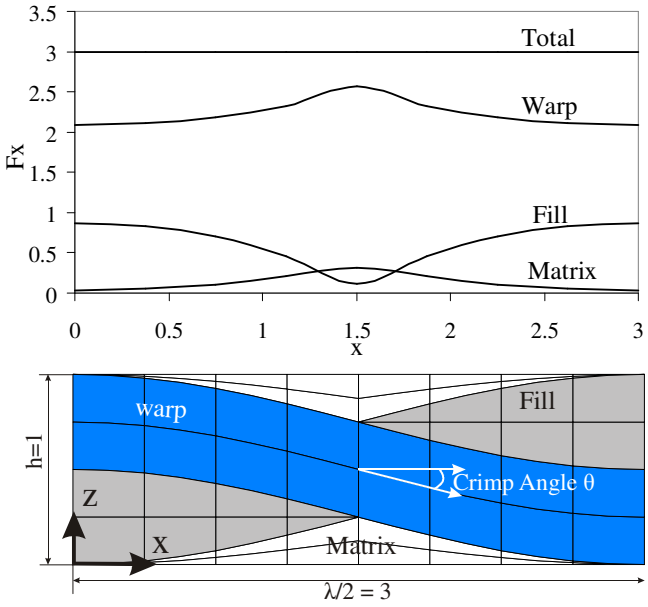

Fig. 6. Fx load distribution in warp/fill & matrix

dip and the load reduces by 86% at the maximum undulation of the warp tow. The load redistribution occurs because at different cross sections of the model along the x-direction, the relative material areas of fill tow and matrix pockets vary (see Fig 6). At x=0, there is very little matrix pocket as compared to at x=1.5, where there is almost no fill tow material. The matrix has much less stiffness as compared to the transverse stiffness of the fill (E=3GPa for matrix versus E_{yy}=22GPa for fill tow). Depending upon the relative areas of matrix and fill tow at any cross-section, load will redistribute between warp, fill and matrix pockets. Hence the warp tow and matrix pick up the load at the maximum undulation region.

This reasoning was validated by investigating a "*stiffened matrix configuration*" in which the matrix shown in Fig. 6 has the same properties as the transverse properties of the tow. When the matrix is stiffened, the Fx in the warp tow decreases by 7.7% (see Fig. 7 (a)) at the point of maximum undulation….in sharp contrast to the 23% increase for the warp tow of regular matrix configuration. In Fig. 6, there are apparently two competing mechanisms. First is the load redistribution into the warp tow as fill tow is replaced by softer matrix. The second is load redistribution out of the warp tow because an inclined tow is not as stiff as a horizontal tow. In Fig. 6, the first is the dominant mechanism. When the matrix is stiffened, the first mechanism is virtually non-existent and the second mechanism

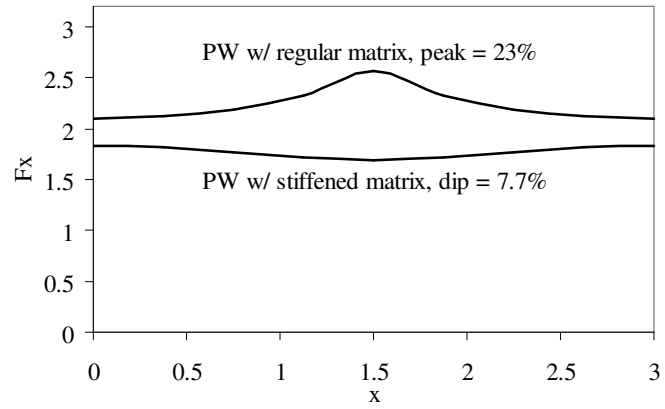

(a) Variation of Fx

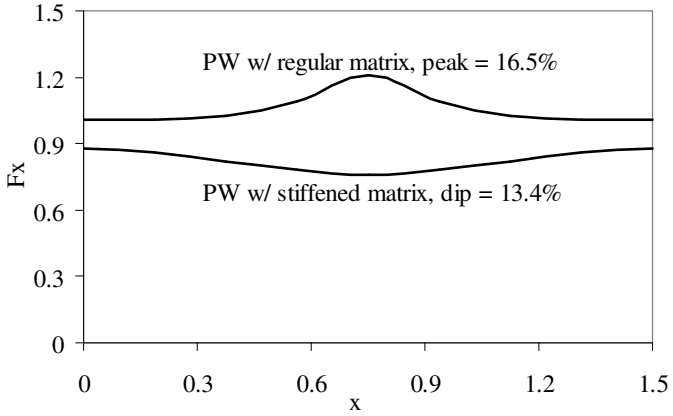

(b) Variation of Fx in configurations with higher undulation (wavelength λ=3)

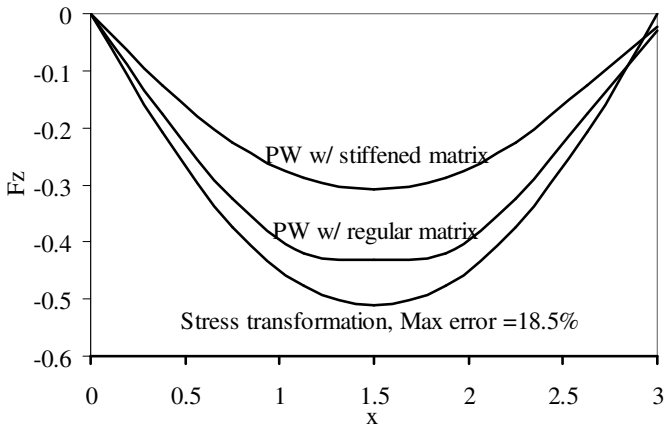

(c) Variation of Fz

Fig. 7. Comparison of load flow in different configurations

results in a reduction in Fx at x=1.5. If we increase the undulation angle (i.e. waviness) by decreasing the wavelength (λ), the load shedding mechanism should become more pronounced. Fig. 7(b) shows the variation of Fx for the PW with the smaller wavelength λ=3. In the case of warp tow of a PW with regular matrix, the load peak at the maximum undulation region dropped to 16.5% (as compared to 23% in the case of less wavy configuration) and in the case of stiffened matrix configuration, the load dip increased to 13.4% (as compared to 7.7% in the case of less wavy configuration). These observations are consistent with the proposed mechanisms.

Figure 7 (c) shows the distribution of out of plane stress resultant Fz along the x direction. The existence and variation of Fz in plain weave can be approximately explained by a simple stress transformation. Let us assume that the only non-zero stress in the warp tow is σ_{11}, which is the normal stress along the axis of the fibers (see Fig. 8). It is also assumed that σ_{11} is constant throughout the warp tow. The average σ_{11} was approximated by dividing the Fx stress resultant at x=0 with the cross-sectional area of the warp tow.

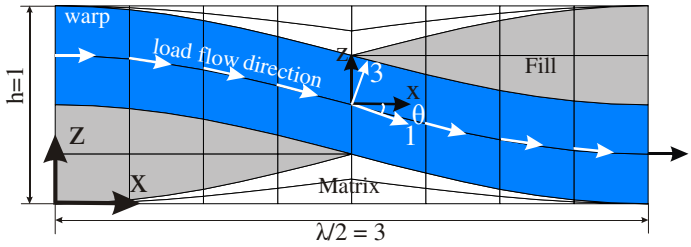

Fig. 8. Load flow direction in warp tow with the coordinate system for stress transformation

This simplified stress state was transformed to the global coordinate system xz. The transformed transverse shear stress is given by:

$$\sigma_{xz} = -\sigma_{11}\cos(\theta)\sin(\theta) \qquad (2)$$

where $\theta = \tan^{-1}\left(\frac{\partial z}{\partial x}\right)$ and $z = \frac{h}{4}\cos\left(\frac{2\pi x}{\lambda}\right)$

The transverse force Fz is simply $A\sigma_{xz}$.

The Fz stress resultant obtained by this simple transformation is also plotted in the Fig. 7(c) as a function of x. It can be seen that the simple formula predicts the trend reasonably well. The maximum difference between the finite element predictions and the simple stress transformation is around 18.5%. Further study is needed to confirm that this agreement is not coincidental. Unlike Fx, whose variation is mainly governed by relative fill and matrix properties, the existence and variation of Fz is due to the warp tow undulation. Hence, the dip at maximum undulation should not disappear even in the case of a stiffened matrix configuration. Fig. 7(c) shows that, in fact, is the case.

4.1.2 Correlation between Stress Resultants & Stress Concentrations

A correlation exists between the variation of the stress resultants and the location of stress concentrations. The regions where stress is concentrated are the potential damage initiation spots. Fig. 9 shows σ_{xx} and σ_{xz} stress contours for the warp tow of a plain weave and curved beam. The *"curved beam configuration"* has only warp tow in space and was used to obtain insights about the behavior of the warp tow of a PW. In Fig. 9, the location of peak stresses is marked by arrows for both configurations.

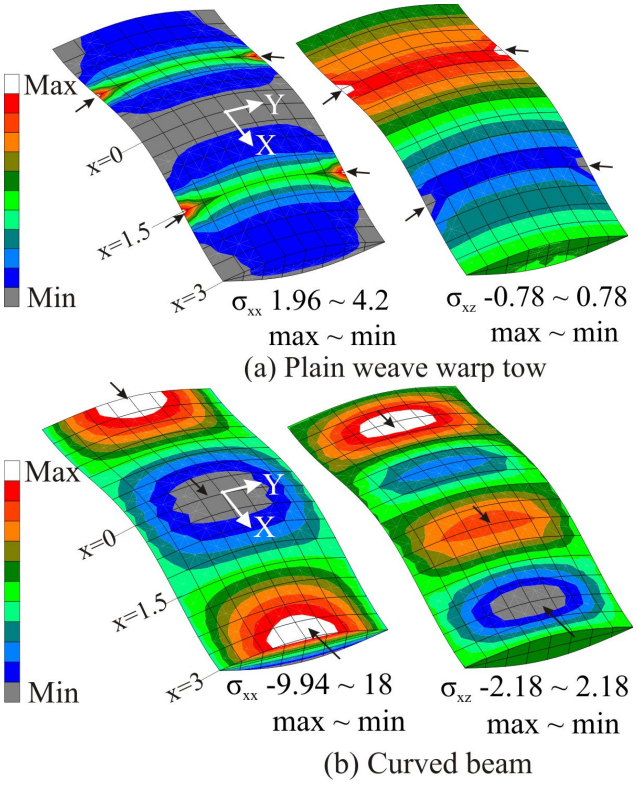

Fig. 9. Stress contours for σ_{xx} and σ_{xz}

Fig. 9 (a) shows that for the warp tow, there is a large variation in σ_{xx} stress. The peak σ_{xx} occurs at the maximum undulation region, which is also the region of peak in Fx in the warp tow. The σ_{xz} stress is also non-uniform throughout the warp tow with a maximum at the maximum undulation region. This is also the region of the maximum Fz, as discussed earlier (Fig. 7 (c)). Hence, a correlation between the magnitudes of stress resultants and location of stress concentrations exists. The correlation between peak stress resultants and peak stresses was also observed for the stiffened matrix configuration.

In the case of a curved beam, though Fx is constant, there is a wide variation in the σ_{xx} stress distribution. In a curved beam, the maximum stress exists in the region of zero crimp because that is the region of maximum bending moment. Variation of Ry bending moment along the length of warp tow and curved beam is shown in Fig. 10. The warp tow has almost zero bending moment, whereas for the curved beam, the moment varies considerably as we move along different cross-sections of the beam. The bending moment is maximum at the zero crimp angle region (i.e. at x=0 and x=3) and zero at the maximum undulation (i.e. at x=1.5), which is expected.

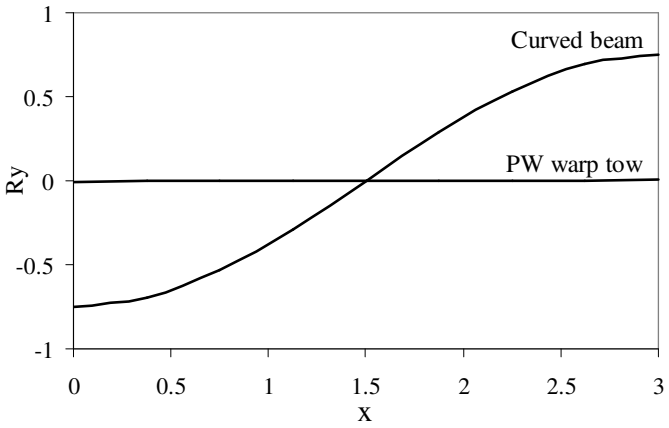

Fig. 10. Comparison of bending moment in PW warp tow and in curved beam

Non-zero bending moment in a curved beam causes almost a linear variation of the σ_{xx} stress in the curved beam, whereas in the warp tow, the variation is not linear. The peak stress locations, magnitudes, stress resultants and bending moment are distinctly different in the warp tow of a plain weave as compared to in a curved beam. These results suggest that one should be careful about approximating the tows as curved beams in approximate models.

4.1.3 Typical Stress Volume Distribution in the Warp Tow of a Plain Weave

Here the stress distributions are analyzed using a stress volume distribution plot for the warp tow of a plain weave. A volume averaged stress $\langle\sigma_{xx}\rangle$=304 MPa was applied to the PW model. It caused a volume averaged strain of $\langle\varepsilon_{xx}\rangle$=1%. Analysis of stress contours in the warp tow shows that the peak σ_{11}, σ_{22}, σ_{33} and σ_{13} stress magnitudes are 0.46, 1.84, 1.27 and 1.7 times their corresponding strengths, respectively. This suggests that σ_{22} is the most critical component for failure initiation. Below we examine a stress volume distribution plot to obtain another perspective.

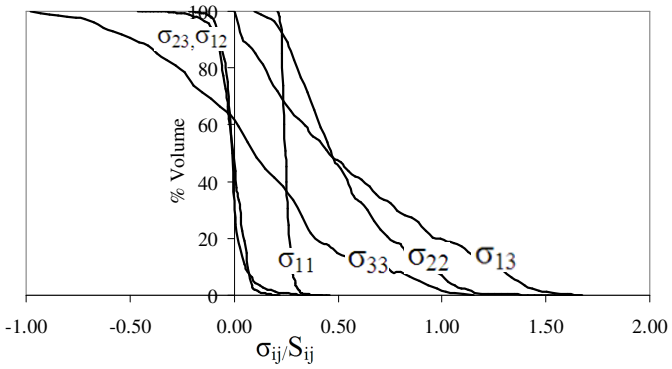

Fig. 11. Stress volume distribution in warp tow (Applied volume averaged $<\sigma_{xx}>$=304 MPa & the stress is normalized by the strength)

Figure 11 shows the stress volume distribution in the warp tow. The distribution is shown for all six stress components. The stresses (σ_{ij}) are normalized with their respective strengths (S_{ij}). This plot reveals how much volume of the material has a stress magnitude larger than a particular value. Assuming a maximum stress failure criterion, one could also find how much volume exceeds a critical stress.

Figure 11 shows that only 1.2% of the volume has σ_{33} stress greater than S_{33}. The σ_{22} peak value is $1.84S_{22}$, but less than 5% of the tow has σ_{22} greater than $1.03S_{22}$. Hence, these stress concentrations are so localized that slight yielding might eliminate the stress concentrations. In contrast, a considerable volume of the tow (about 19%) has σ_{13} greater than S_{13}. This means that a considerable volume of the tow is highly stressed and might cause failure initiation under this mode. Thus, σ_{13} might be the most critical stress component unlike initially suggested by analysis of stress contours.

4.2 Effect of Textile Architecture on Stress Resultants

Here the effect of weave architecture on the variation of stress resultants along the length of a warp tow was considered. To have meaningful comparisons, comparable regions were identified and analyzed. The comparable regions are shown in Fig 3. Mesh refinement was the same for the different weave architectures. In this section, the variation of stress resultants is compared for the warp tow present in comparable regions. Meshes for different weave architectures are shown in Fig. 3. Figures 12, 13 and 14 show the effect of weave architecture on the variation of stress resultants in the warp tow.

In the comparable regions, all the weaves show a similar peak in Fx at the maximum undulation region (see Fig. 12). The distribution for PW and Twill is symmetric while for satin weaves, it is not. This is due to the fact that PW is symmetric and Twill weave is anti-symmetric whereas others are not (see Figure 3(b)). The Fz distributions (see Fig. 13) are also very similar to each other for different weaves. Hence, in terms of Fx and Fz stress resultants, the global architecture has little effect on the warp tow in the local comparable regions.

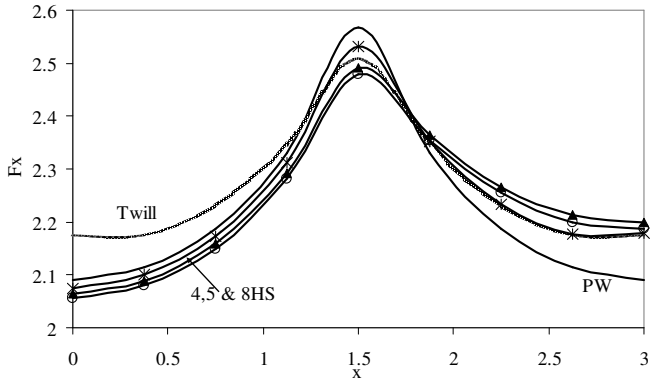

Fig. 12. Effect of weave architecture on Fx distribution in the warp tow

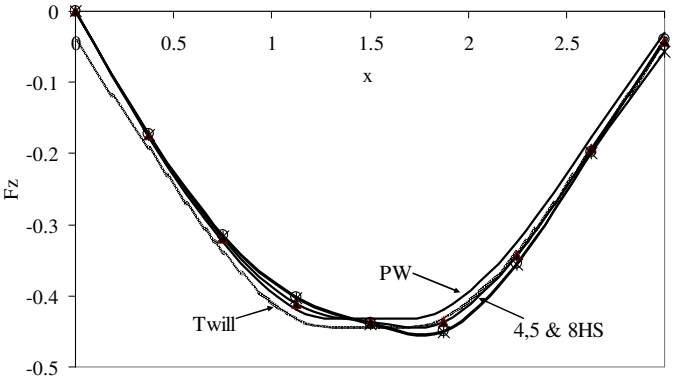

Fig. 13. Effect of weave architecture on Fz distribution in the warp tow

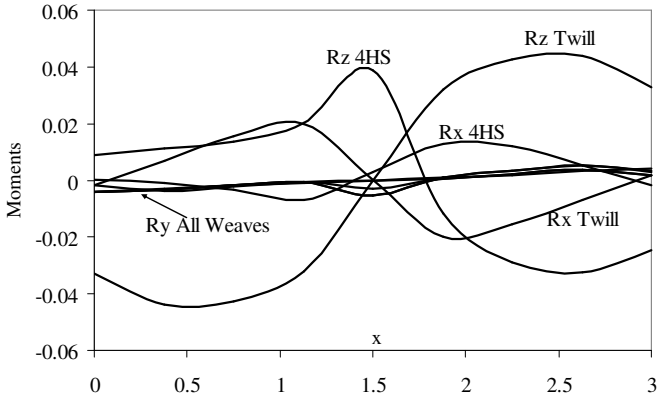

Fig. 14. Effect of weave architecture on variation of moments in the warp tow

The observations are different in the case of moment distribution, which is shown in Fig. 14. If non-zero stress resultants Fx or Fz do not act through the center of the cross-section of the tow, then it will result in non-zero moment at that cross-section of the tow. All the architectures have non-zero out of plane bending moment Ry. But this out of plane bending is very small for all the cases as shown in Fig. 14. Twill and 4HS have significant non-zero in plane bending Rz and out of plane bending Rx. Although nodal forces in the y- and z directions contribute to the Rx moment, the nodal forces in the y-direction were negligibly small, hence their contribution to the Rx moment was also negligibly small.

The y offsets between the lines of action of stress resultants Fx and Fz and the xz plane are referred to as y_{Fx}^{off} and y_{Fz}^{off} respectively herein. It must be noted that the moment is a combined measure of offsets and magnitude of the force stress resultants. The moment at any cross-section will be zero if either of those is zero. Both y_{Fx}^{off} and y_{Fz}^{off} are non-zero at most of the warp tow cross-sections of the Twill and 4HS weaves. The existence of y_{Fx}^{off} only for Twill and 4HS weaves and not for others, can be explained by carefully examining the architecture of different weaves. Figure 3(b) shows the weave architectures in the comparable regions. For Plain, 5HS and 8HS weaves, y=0 is a plane of symmetry. For Twill weave, there is no symmetry about y=0. For 4HS, there is no symmetry about y=0 for half of the comparable region from x=1.5 to x=3. For the rest of the comparable region, the 4HS weave is symmetric about y=0.

Now if we examine the cross-section of the twill model at x=3 (refer Fig. 3(b)), we can see that the left half has fill tow woven around the warp tow whereas the right half has a gap (filled by matrix) between the fill and warp. This causes better reinforcement of the warp on the left half than on the right half. Hence, the right half of the warp tow has to take more Fx load than the left half. This causes Fx to shift to the right (positive y direction) for the warp tow cross-section at x=3. If this hypothesis is true, then the following should also be true for the Twill weave:

- Warp tow should have negative y offset in Fx at cross-section x=0.
- Fill tow should have opposite offsets in Fx as compared to warp tow offsets at each cross-section.
- Offset in Fx for warp/fill tow should disappear for stiffened matrix configuration.

Figure 15 shows that this is the case. In Fig. 15, the bending moment Rz for warp and fill tows of the Twill weave is shown. From x=0 to x=1.5, the warp tow has negative Rz due to the presence of gaps in warp and fill in the negative y direction. Also, the variation of Rz is anti-symmetric about x=1.5 since the architecture of the twill weave is anti-symmetric. The fill tow has an opposite moment distribution as compared to the warp tow. Figure 15 also shows that Rz for the warp tow of a stiffened matrix configuration is very small. Since Fx for each cross-section is considerably large, y_{Fx}^{off} for warp tow was calculated to be negligible for the stiffened matrix configuration.

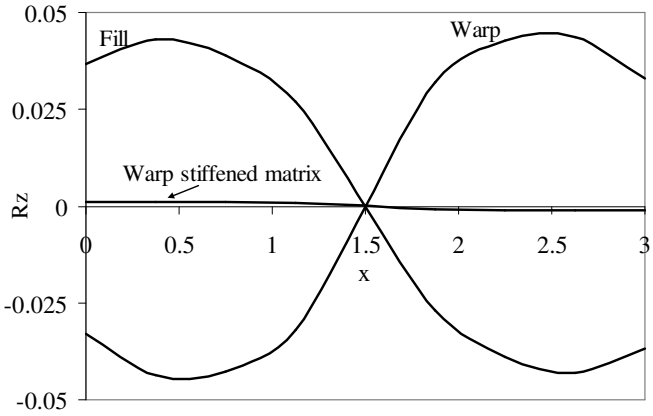

Fig. 15. Variation of R_x^y for warp, fill and matrix.

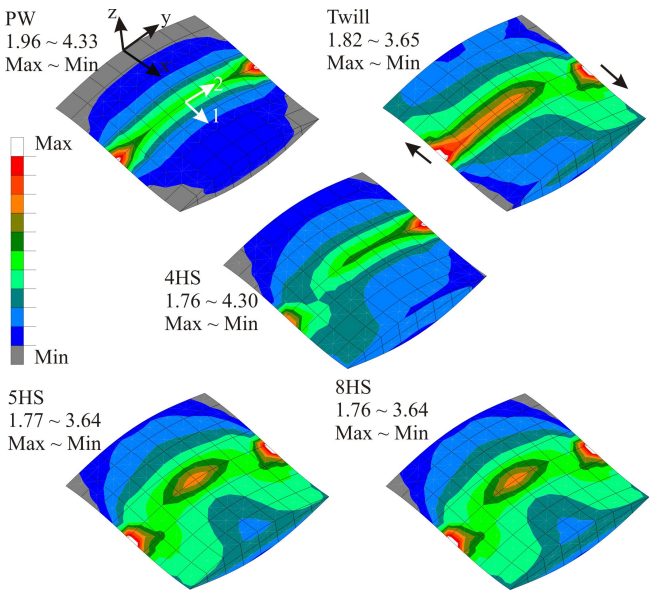

Fig. 16. The σ_{11} contours in comparable regions of the warp tow for different architectures.

The effect of offset of Fx on the location of σ_{11} stress concentrations was also examined. Figure 16 shows the σ_{11} contours in comparable regions of the warp tow for different architectures. For PW, 5HS and 8HS weaves the stress contours are symmetric about the plane y=0. The stress concentrations are located at the maximum undulation regions and near both edges of the tow. For the case of Twill and 4HS weaves, the stress contours are not symmetric. For Twill weave, the stress concentrations are shifted slightly, as indicated by arrows in Fig. 16. This shift in locations of stress concentrations might be caused by the Fx offset. Since there is negligible Fx offset for a stiffened matrix twill weave configuration, the σ_{11} stress contours are "pretty much" symmetric about y=0 plane as shown by Fig. 17.

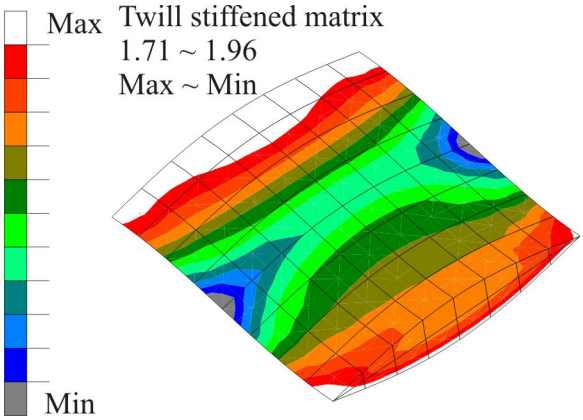

Fig. 17. The σ_{11} contours in the warp tow of the stiffened matrix twill weave configuration

5 Conclusions

The main observations of this paper are summarized as follows:

- Increase in computational power has made detailed three-dimensional finite element analyses practical, but special post-processing techniques are required to interpret the massive amount of data.
- In the warp tow of a plain weave, maximum axial and transverse loads occur at the maximum undulation region. This is due to the load redistribution in warp, fill and matrix, which in turn occurs because the distribution of fill and matrix material around the warp tow varies along the tow path.
- The existence and variation in transverse load can be explained by using a simple stress transformation.
- There is a correlation between the locations of stress concentrations and locations of peak stress resultants.
- The stress state in the warp tow is non-uniform and fully three dimensional. Some stress concentrations might be so localized that slight yielding might significantly reduce those stress concentrations.
- In comparable regions, all the weaves show a similar peak in the axial and transverse stress resultants at the maximum undulation region.
- In contrast, significant differences in bending moments exist. The lack of symmetry in Twill and 4HS weaves causes offset of the force stress resultants from the centroid of the tow cross-section.

6 Acknowledgements

This work was supported by the Texas Institute for Intelligent Bio-Nano Materials and Structures for Aerospace Vehicles, funded by NASA Cooperative Agreement No. NCC-1-02038. Any opinions, findings and conclusions or recommendations expressed in this material are those of the authors and do not necessarily reflect the views of the National Aeronautics and Space Administration

References

[1] Paumelle P., Hassim A. and Léné F. "Composites with woven reinforcements: calculation and parametric analysis of the properties of homogeneous equivalent". *La Recherche Aérospatiale*, Vol. 1, pp 1-12, 1990.

[2] Whitcomb J. D. "Three-dimensional stress analysis of plain weave composites". NASA TM 101672, *Composite Materials: Fatigue and Fracture*, Third Volume, T.K. O'Brien, ed., ASTM STP 1110, pp. 417 438, 1991

[3] Ishikawa T. and Chou T. W. "Elastic behavior of woven hybrid composites". *Journal of Composite Materials*, Vol. 16, pp 2–19, 1982

[4] Naik N. K. and Shembekar P. S., "Elastic behavior of woven fabric composites: I - Lamina analysis". *Journal of Composite Materials*, Vol. 26, pp.2196-2225, 1992

[5] Whitcomb J. D., Chapman C. D. and Tang X. "Derivation of boundary conditions for micromechanics analyses of plain and satin weave composites". *Journal of Composite Materials*, Vol. 34, No. 9, pp. 724-769, 2000.

[6] Chamis C. C., "Simplified composite micromechanics equations for strength, fracture toughness, impact resistance and environmental effects". *Technical memo. access number ADA304541*, NASA Cleveland OH Lewis Research Center, pp 1-28, 1984.